International Journal of Electrical, Energy and Power System Engineering
Vol. 09, No. 03, October 2026
e-ISSN: 2654-4644

Feasibility Aware PV BESS Co-Planning with Cyclic Dispatch Repair in Radial Distribution Networks

Trieu Ngoc Ton*
Thu Duc College of Technology, Ho Chi Minh, Vietnam, tonngoctrieu@gmail.com

*Corresponding author, tonngoctrieu@gmail.com

Abstract— This study investigates a feasibility aware co-planning framework for photovoltaic (PV) generation and a battery energy storage system (BESS) in radial distribution networks (DNs). The framework jointly determines the locations and capacities of three PV units, the location and energy rating of one BESS, and its 24 hour operating schedule using a normalized five criterion objective covering daily energy losses, voltage deviation, accommodated PV capacity, renewable curtailment, and branch current utilization. Cyclic BESS dispatch repair is combined with hourly backward/forward sweep power flow and feasibility first selection to enforce battery, voltage, and thermal constraints. The Multi Verse Optimizer (MVO), Differential Evolution (DE), Harris Hawks Optimization (HHO), and Artificial Rabbits Optimization (ARO) are compared under a common budget of 3,000 evaluations and 30 independent runs, with a 0.90–1.05 p.u. voltage band adopted because the evening peak cannot satisfy 0.95 p.u. with unity power factor units. For the IEEE 33 bus and 69 bus systems, all 240 runs are feasible; the best solutions accommodate up to 2.85 and 3.30 MW of PV and reduce daily losses from 3.405 to 2.221–2.365 MWh and from 3.768 to 2.344–2.605 MWh, depending on the algorithm. ARO and DE attain the lowest mean objective values, with the differences remaining significant after Holm correction; cyclic repair proves essential for terminal-energy feasibility. The reported PV capacities represent the best feasible solutions found within the computational budget rather than certified hosting capacity limits; the supporting data workbook is provided for independent verification.

Keywords: Battery storage, Cyclic battery schedule, Multi-verse optimizer, Operational feasibility, Photovoltaic accommodation.

This work is licensed under a CC BY-NC. Copyright ©2026 by Author. Published by Universitas Riau.

INTRODUCTION

The growing penetration of photovoltaic (PV) generation in radial distribution networks (DNs) introduces voltage rise, reverse power flow, thermal congestion, and renewable energy curtailment [1], [2]. These challenges constrain the amount of PV generation that can be safely accommodated without network reinforcement. Battery energy storage systems (BESSs) can mitigate these effects by shifting energy across operating periods; however, their benefits depend on the coordinated selection of PV locations and capacities, BESS placement and size, and charging/discharging schedules. Joint planning is therefore

Received: June 28, 2026, Revised: Aug 23, 2026, Accepted: Oct 31, 2026
https://doi.org/10.31258/ijeepse.9.3.202-220

essential for improving renewable accommodation while preserving network security [3], [4].

Existing PV–BESS planning studies have applied mathematical programming and population-based optimization to reduce losses, improve voltage profiles, or increase renewable integration. Nevertheless, three methodological issues remain important [5], [6]. First, long-term siting and sizing decisions are not always evaluated jointly with the full time-coupled battery schedule [7], [8]. Second, penalty-based optimization may retain attractive but infeasible candidates when state of charge (SOC), terminal energy, voltage, or thermal limits are violated [9]. Third, the installed PV capacity of a feasible solution is sometimes described as the network's maximum hosting capacity (HC), although such a global claim requires a separate capacity-limit verification [9], [10]. These issues motivate a planning framework in which battery feasibility and network feasibility are explicitly checked at every operating interval.

This paper presents a feasibility-aware PV BESS co-planning framework for radial DNs [11], [12]. The proposed approach jointly optimizes the locations and capacities of three PV units, the placement and energy rating of one BESS, and its 24-hour operating schedule. A cyclic BESS dispatch repair procedure is integrated with hourly backward/forward sweep power flow assessment and feasibility first selection to address battery and network operating constraints. The resulting accommodated PV capacity is interpreted as the installed capacity of the best feasible solution identified within the computational budget rather than a globally certified HC limit [13], [14].

The Multi-Verse Optimizer (MVO) is used as the reference search method [15], [16] with Differential Evolution (DE) [17], [18], Harris Hawks Optimization (HHO) [19], [20], and Artificial Rabbits Optimization (ARO) [21], [22] as benchmarks under common decision variables, constraints, and evaluation budgets. The novelty lies in the integrated formulation and constraint handling workflow, which is algorithm agnostic, rather than in new search operators; the four optimizers are therefore compared within the same framework. The contributions are:

(i) A joint discrete continuous PV BESS planning model coupled to 24 hour operation;

(ii) Cyclic battery dispatch repair followed by network level feasibility screening;

(iii) A consistent renewable accommodation metric and comparative evaluation using independent runs, statistical tests, and component-wise ablation.

The framework is assessed on the 33 bus and 69 bus radial systems using hourly load and PV profiles. Performance indicators include feasible installed PV capacity, energy losses, voltage and current limits, renewable curtailment, grid imports, and daily grid electricity purchasing expenditure under time of use (TOU) tariffs. The expenditure metric does not represent a complete life cycle cost because investment, degradation, replacement, and maintenance costs are excluded. The remainder of the paper presents the mathematical model, solution procedure, experimental setup, results and discussion, and conclusions.

METHOD

A. Distribution Network Power Flow Model

The proposed framework considers a balanced radial DN with N_b buses and N_l branches. Three PV units and one BESS are jointly planned over a 24 hour scheduling horizon. Hourly operating conditions are evaluated using backward/forward sweep (BFS) power flow [23] with base quantities of 12.66 kV and 10 MVA. Bus 1 is the slack bus. The benchmark active and reactive load demands are scaled using the hourly factors in Table 4. At buses without PV or

BESS, the corresponding injections are zero. A positive BESS injection represents discharge, whereas a negative value represents charging; PV and BESS are modeled at unity power factor.

$$P_i^{net}(t) = P_{L,i}(t) - P_{PV,i}(t) - P_{B,i}(t) \quad (1)$$

$$Q_i^{net}(t) = Q_{L,i}(t) \quad (2)$$

In (1) and (2), the active and reactive load demands at bus *i* and hour *t* are expressed in MW and MVAr, respectively. The utilized PV power and BESS power are expressed in MW. Positive BESS power denotes discharging, whereas negative power denotes charging. At buses without PV or BESS installations, the corresponding power injections are zero. Both PV and BESS are assumed to operate at unity power factor. Active power loss and daily energy loss are:

$$P_{loss}(t) = \sum_{l=1}^{N_l} R_l \left|I_l(t)\right|^2, \; E_{loss} = \sum_{t=1}^{T} P_{loss}(t)\Delta t \quad (3)$$

where the branch resistance and current must be expressed in consistent electrical units, $T = 24$, and $\Delta t = 1\,h$. The mean voltage deviation is:

$$VD = \frac{1}{N_b T} \sum_{t=1}^{T} \sum_{i=1}^{N_b} \left| \left|V_i(t)\right| - 1 \right| \quad (4)$$

For the network performance indicators, N_I and N_b denote the numbers of branches and buses; R_I is the resistance of branch l, $I_l(t)$ its complex current magnitude, and $V_i(t)$ the per unit voltage magnitude at bus i. E_{loss} is the total energy dissipated over the scheduling horizon, whereas VD measures the average absolute departure of the voltage profile from 1.0 p.u. The adopted current and resistance bases must be consistent: for a balanced three phase equivalent, branch losses in physical units are computed with the corresponding three phase convention.

B. PV Generation and Accommodated Capacity

The PV model separates available generation from the energy actually injected into the network. This distinction is required because the nominal installed capacity alone does not determine the usable renewable production under voltage, current, and storage limitations.

$$P_{PV,j}^{av}(t) = P_{PV,j}^{r} G(t) \quad (5)$$

$$P_{PV,j}(t) = P_{PV,j}^{av}(t)[1 - \gamma(t)] \quad (6)$$

where $G(t) \in [0, 1]$ is the normalized PV output factor and $\gamma(t) \in [0, 1]$ is the common hourly curtailment fraction. The curtailed, utilized, and available daily PV energies are

$$E_{curt} = \sum_{t=1}^{T} \sum_{j=1}^{N_{PV}} \gamma(t) P_{PV,j}^{av}(t)\Delta t \quad (7)$$

$$E_{use} = \sum_{t=1}^{T} \sum_{j=1}^{N_{PV}} (1 - \gamma(t)) P_{PV,j}^{av}(t)\Delta t \quad (8)$$

$$RU = 1 - \frac{E_{curt}}{E_{PV}^{av}} \quad (9)$$

$$E_{PV}^{av} = \sum_{t=1}^{T} \sum_{j=1}^{N_{PV}} P_{PV,j}^{av}(t)\Delta t \quad (10)$$

The available, utilized, and curtailed PV energies are calculated over the 24-hour scheduling horizon and expressed in MWh. Renewable utilization (RU) represents the ratio of utilized PV energy to available PV energy. This ratio is evaluated when the available PV energy is positive; otherwise, a predefined convention is applied to avoid division by zero. The PV capacity accommodated by a particular feasible solution is

$$HC_{sol} = \sum_{j=1}^{N_{PV}} P_{PV,j}^{r} \quad (11)$$

The accommodated PV capacity in (11) represents the total installed PV capacity of a feasible solution, expressed in MW. A candidate is considered feasible only when its 24-hour power flow results and BESS operating trajectory satisfy the prescribed constraints. Therefore, the reported accommodated capacity corresponds to the best feasible solution identified by the optimization algorithm within the specified computational budget, rather than a mathematically certified maximum HC limit.

C. BESS Model

The BESS is modeled through an intertemporal energy balance that accounts for charging and discharging efficiencies. Unlike instantaneous operating constraints, its state of charge depends on all preceding charging and discharging decisions. Consequently, optimizing each hour independently would not preserve the energy feasibility of the complete daily schedule.

$$E_B(t+1) = \{E_B(t) - \frac{P_B(t)\Delta t}{\eta_d},\ P_B(t) \geq 0,\ E_B(t) - \eta_c P_B(t)\Delta t,\ P_B(t) < 0 \quad (12)$$

$$SOC(t) = \frac{E_B(t)}{E_B^r} \quad (13)$$

In (12) and (13), the stored battery energy at the beginning of hour t and the rated BESS energy capacity are expressed in MWh, while the BESS charging/discharging power is expressed in MW. During charging, the stored energy increases according to the charging efficiency, whereas during discharging, it decreases according to the discharging efficiency. The 24-hour scheduling horizon comprises 24 control intervals and 25 battery energy state boundaries. The battery operational limits and the cyclic requirement are:

$$SOC_{min} \leq SOC(t) \leq SOC_{max} \quad (14)$$

$$-P_B^{ch,max} \leq P_B(t) \leq P_B^{dis,max} \quad (15)$$

$$SOC(T+1) = SOC(1) \quad (16)$$

The nominal settings are $SOC_{min} = 0.20$, $SOC_{max} = 0.90$, $SOC(1) = 0.50$, and $\eta_c = \eta_d = 0.95$.

The cyclic condition in (16) enforces equal energy at the beginning and end of the daily horizon and prevents a solution from appearing beneficial by simply emptying the battery. SOC limits are imposed at every state boundary, including the terminal state. Charging and discharging cannot occur simultaneously because a single signed BESS power variable is used in each hourly interval.

D. Normalized Multi-criteria Objective

A normalized scalar objective is used to compare candidate solutions consistently while retaining the technical meaning of its five components. All terms are minimized, and fixed nonnegative weights are applied identically to every algorithm.

$$\min_{x} F(x) = \sum_{k=1}^{5} w_k f_k(x) \tag{17}$$

$$f_1 = \frac{E_{loss}}{E_{loss}^0},\ f_2 = \frac{VD}{VD^0},\ f_3 = 1 - \frac{HC_{sol}}{P_{PV}^{max}},\ f_4 = \frac{E_{curt}}{E_{PV}^{av}},\ f_5 = \frac{1}{N_l T}\sum_{l=1}^{N_l}\sum_{t=1}^{T}\frac{|I_l(t)|}{I_l^{max}} \tag{18}$$

$$w = [0.25,\ 0.15,\ 0.25,\ 0.15,\ 0.20],\ \sum_{k=1}^{5} w_k = 1,\ w_k \geq 0 \tag{19}$$

E_{loss}^0 and VD^0 are calculated from the same 24 hour base-case profile without PV BESS. P_{PV}^{max} is the prescribed aggregate PV planning bound, not an established maximum HC. The weights represent planning preferences; sensitivity testing is required to assess the effect of alternate choices. The fifth criterion measures normalized average feeder loading, not the minimum branch headroom.

In the normalized multi criteria objective formulation, F denotes the total dimensionless objective value, and w_k denotes the nonnegative weighting coefficient assigned to criterion k.

The first component measures the daily loss relative to the no PV BESS baseline; the second compares average voltage deviation with its baseline; the third rewards a larger accommodated PV capacity relative to the exogenously specified planning ceiling. The fourth is the fraction of available PV energy curtailed, and the fifth is the mean branch current utilization relative to its thermal rating. These quantities should not be conflated with an exact network HC boundary, a branch safety margin minimum, or a total life cycle cost.

E. Decision Variables and Constraints

The decision vector is

$$x = \left[L_{PV},\ P_{PV}^r,\ L_B,\ E_B^r,\ P_B,\ \gamma\right] \tag{20}$$

The optimization model comprises 56 decision variables, including four discrete location variables and 52 continuous variables. The discrete variables specify the installation buses of three PV units and one BESS, while the continuous variables consist of three PV capacities, one BESS energy capacity, 24 hourly signed BESS power values, and 24 common PV curtailment ratios. Positive BESS power represents discharging, whereas negative power represents charging. The SOC trajectory is calculated using the intertemporal energy-balance equation. Discrete location variables are decoded before numerical simulation, and duplicate PV locations are repaired consistently across all algorithms.

Table 1 specifies the decision variable and operating constraints, and Table 2 lists the numerical limits. The uniform 255 A thermal limit is a simulation assumption and should not be described as a verified rating for each physical conductor. The aggregate PV capacity is limited to 2.85 MW and 3.30 MW for the 33-bus and 69-bus networks, respectively. The same BESS capacity, charging/discharging power, voltage, and branch current limits are applied to all optimization algorithms.

For the investigated benchmark scenario, a study-specific lower voltage limit of 0.90 p.u. is adopted because, with unity power factor PV and BESS units and the converter ratings in

Table 1. Decision Variables and Operational Constraints

Quantity	Admissible range or requirement
PV locations	Three distinct admissible non-slack buses
PV capacities	$0 \leq P^{r}_{PV,j} \leq P^{max}_{PV,j}$
BESS location	One admissible non-slack bus
BESS energy capacity	$E^{min}_{B} \leq E^{r}_{B} \leq E^{max}_{B}$
BESS power	Equation (15)
PV curtailment	$0 \leq \gamma(t) \leq 1$
SOC	$0.20 \leq SOC(t) \leq 0.90$
Cyclic SOC	$SOC(25) = SOC(1) = 0.50$
Voltage	$0.90 \leq \lvert V_i(t) \rvert \leq 1.05$ p.u.
Branch current	$\lvert I_l(t) \rvert \leq I^{max}_{l}$

Table 2, the evening peak load hours (19:00–21:00, zero PV output) cannot satisfy 0.95 p.u. even with full BESS discharge at the most favorable bus: the maximum attainable minimum voltage is 0.925 p.u. for the 33 bus system and 0.938 p.u. for the 69 bus system. Reactive power support from the inverters is outside the scope of this study. Therefore, the adopted voltage band is a simulation assumption for the investigated benchmark cases and should not be interpreted as a universal distribution network operating standard.

Table 2. Network, Planning, and BESS Parameters of the Investigated Systems

Parameter	IEEE 33-bus	IEEE 69-bus
Number of buses / branches	33 / 32	69 / 68
Total peak load (kW / kvar)	3,715 / 2,300	3,802.2 / 2,694.1
Nominal voltage (kV) / base power (MVA)	12.66 / 10	12.66 / 10
PV units / BESS units	3/1	3/1
Maximum per-PV rating (MW)	0.95	1.10
Aggregate PV planning limit (MW)	2.85	3.30
BESS energy capacity range (MWh)	0.20–1.80	0.20–2.00
Maximum charge/discharge power (MW)	0.55	0.65
Voltage limits (p.u.)	0.90–1.05	0.90–1.05
Uniform assumed current limit (A)	255	255
SOC limits / initial = terminal SOC (%)	20–90 / 50	20–90 / 50
Charge/discharge efficiency (%)	95 / 95	95 / 95
Scheduling horizon (h)	24	24

F. Daily Grid Electricity Purchasing Expenditure

In addition to the technical criteria in (17)–(19), the economic effect of the PV BESS configuration on the distribution company is assessed through the cost of electricity purchased from the upstream grid. This indicator is not included in the objective function; it is evaluated after optimization for the best solution of each algorithm, using the hourly substation import obtained from the 24 hour BFS results and the TOU tariff in Table 6. Because the tariff periods change at 09:30 and 11:30, a time weighted average tariff is applied to the hourly intervals that cross these transitions. The post optimization cost indicator is

$$C_{grid} = \sum_{t=1}^{T} \pi(t) P_{import}(t) \Delta t \quad (21)$$

Here, $\pi(t)$ is the TOU electricity tariff and $P_{import}(t)$ is nonnegative upstream grid import. This measure is daily grid electricity purchasing expenditure, not full life cycle cost; BESS investment, maintenance, replacement, and degradation are excluded. In (21), $\pi(t)$ denotes the hourly electricity purchase tariff (USD/kWh), $P_{import}(t)$ is nonnegative imported active power (kW), and Δt is the interval duration in hours. If the power flow solver returns MW, multiplying by 1000 is required before applying a USD/kWh tariff. Reverse power flow at the substation, if any, is reported separately as exported energy and is not credited. The resulting indicator is daily grid electricity purchasing expenditure, not total operating cost or discounted project cost.

G. Solution Procedure

The solution procedure integrates candidate decoding, bound projection, time coupled BESS schedule repair, hourly BFS feasibility assessment, and feasibility first selection. The standard MVO search operators are retained, while the proposed constraint-handling procedure is incorporated into candidate evaluation. Each solution is decoded according to the decision vector in (20), with discrete installation locations mapped to admissible buses and duplicate PV locations resolved through deterministic reassignment. Continuous decision variables are subsequently projected onto their prescribed bounds using (22). The hourly charging and discharging limits are determined using (23)–(26), and the terminal battery energy residual is calculated using (27).

$$x_k^{rep} = min\left\{x_k^{max}, max\left[x_k^{min}, x_k\right]\right\} \quad (22)$$

Equation (22) projects continuous decision variables onto their lower and upper bounds. Discrete installation indices are mapped to admissible non slack buses; duplicate PV locations are corrected by deterministic reassignment. These repairs enforce representation bounds only and do not establish battery or network feasibility. For each hour, the feasible discharge and charge magnitudes are determined by the remaining usable energy:

$$P_B^{dis,feas}(t) = min\left[P_B^{dis,max}, \frac{\eta_d\left[E_B(t) - E_B^{min}\right]}{\Delta t}\right] \quad (23)$$

$$P_B^{ch,feas}(t) = min\left[P_B^{ch,max}, \frac{E_B^{max} - E_B(t)}{\eta_c \Delta t}\right] \quad (24)$$

$$E_B^{min} = SOC_{min} E_B^r, \qquad E_B^{max} = SOC_{max} E_B^r \quad (25)$$

$$-P_B^{ch,feas}(t) \le P_B^{rep}(t) \le P_B^{dis,feas}(t) \quad (26)$$

In (23)–(26), $P_B^{dis,feas}(t)$ and $P_B^{ch,feas}(t)$ denote the largest discharge and charge magnitudes allowed by both the converter ratings and the energy remaining within the SOC limits. E_B^{min} and E_B^{max} are the admissible stored energy bounds derived from the rated energy capacity and allowable SOC interval. These hour by hour bounds depend on the state carried forward from the preceding hour, making the repair procedure time coupled. The terminal energy residual is

$$\varepsilon_E = E_B(T + 1) - E_B(1) \quad (27)$$

The terminal energy residual in (27), expressed in MWh, measures the deviation between the final and initial BESS energy states. To minimize this residual, a common adjustment to the signed BESS power schedule is iteratively determined using bisection, followed by sequential SOC projection while accounting for charging and discharging efficiencies. If the prescribed tolerance cannot be achieved, a zero power BESS schedule is adopted as a cyclic feasible fallback, provided that the initial SOC satisfies its operating limits. In either case, the resulting candidate is subjected to the complete 24 hour BFS power flow assessment to verify network feasibility. Voltage and branch current violations are calculated as

$$CV_V = \sum_{t=1}^{T} \sum_{i=1}^{N_b} \left[max\left(0, V_{min} - \left|V_i(t)\right|\right) + max\left(0, \left|V_i(t)\right| - V_{max}\right)\right] \quad (28)$$

$$CV_I = \sum_{t=1}^{T} \sum_{l=1}^{N_l} max\left(0, \frac{\left|I_l(t)\right|}{I_l^{max}} - 1\right) \quad (29)$$

$$CV(x) = CV_V + CV_I + \frac{\left|\varepsilon_E\right|}{E_{ref}} \quad (30)$$

$$CV(x) \leq \varepsilon_{feas} \quad (31)$$

where $E_{ref} = max\left(0.1, E_B^r\right)$ MWh, and $\varepsilon_{feas} = 10^{-7}$ in the implementation. The inequality is applied only if BFS converges and all hard decision bounds are met. CV is a computational ranking measure, not a physical quantity. Feasible solutions outrank infeasible ones; infeasible solutions are compared by CV; feasible solutions are ranked by $F(x)$.

In MVO, each candidate solution is represented as a universe, and the population is updated through white hole/black hole exchanges and wormhole-based exploitation. The wormhole existence probability (WEP) and traveling distance rate (TDR) govern the search process, as defined in (32) and (33). The proposed framework retains the conventional MVO updating mechanism while incorporating feasibility-aware evaluation and selection to ensure that candidate solutions satisfy the prescribed network and BESS operating constraints.

$$WEP(k) = WEP_{min} + k\frac{WEP_{max} - WEP_{min}}{K} \quad (32)$$

$$TDR(k) = 1 - \left(\frac{k}{K}\right)^{1/p} \quad (33)$$

where $WEP_{min} = 0.2$, $WEP_{max} = 1.0$, and $p = 6$. In (32) and (33), k and K denote the current and maximum iteration counts, respectively; WEP represents the wormhole existence probability, TDR denotes the traveling distance rate, and p is the exploitation accuracy exponent. These parameters regulate the exploration-exploitation balance of MVO. Following each population update, candidate solutions undergo the prescribed repair and feasibility assessment procedures. The best feasible solution is retained throughout the search. For comparative evaluation, DE, HHO, ARO, and MVO employ identical decision variables, objective functions, operating constraints, and computational budgets. DE uses the rand/1/bin scheme (F = 0.5, CR = 0.9), whereas HHO and ARO use their standard operators. Each run uses a fixed random seed (10000·Nb + run index), and identical seeds are used for all algorithms. Table 3 summarizes the comparative algorithmic settings applied to DE, HHO, ARO, and MVO, including population size, evaluation budget, number of independent runs, decision variable count, and scheduling horizon.

Step 1 : Load DN topology, nodal loads, hourly PV and demand profiles, TOU tariffs, decision limits, and random seeds.

Step 2 : Initialize a population of 56-dimensional PV BESS solutions.

Step 3 : Decode locations, clip continuous bounds, and restore distinct PV buses.

Step 4 : Apply the hourly BESS power/SOC correction and cyclic schedule repair.

Step 5 : Run hourly BFS, then calculate voltage/current violations and the five objective components.

Step 6 : Rank candidates by feasibility first selection and update the population using the chosen optimizer.

Step 7 : Repeat Steps 3–6 until the fixed evaluation budget is exhausted.

Step 8 : Save the best feasible decision vector, PV BESS dispatch, node voltages, branch currents, grid imports, losses, and curtailed energy.

Step 9 : Repeat for all independent seeds and benchmark methods, and export summary tables, raw results and figures.

Table 3. Comparative Optimization Settings

Parameter	DE	HHO	ARO	MVO
Population size	30	30	30	30
Evaluations per run	3,000	3,000	3,000	3,000
Independent runs	30	30	30	30
Decision variables	56	56	56	56
Horizon (h)	24	24	24	24

Thirty independent runs per algorithm and feeder are summarized using best, mean, median, worst, standard deviation, and elapsed time. MVO and each benchmark are compared using a two-sided Mann Whitney U test on the feasibility-first ranking key (F for feasible runs, 1000 + CV otherwise) with Holm correction across the three comparisons ($\alpha = 0.05$). Statistical significance reflects differences in sampled solution distributions and does not establish global optimality.

To support reproducibility, the Supplementary Data workbook provides the network bus and branch data, 24 hour load and PV profiles, algorithm settings, random seeds, results and 56 variable decision vectors for all independent runs, hourly PV BESS dispatch and SOC trajectories, bus voltages, branch currents, energy balances, and computational times. These archived data allow the reported tables, operating trajectories, statistical summaries, and energy balances to be independently checked.

RESULT AND DISCUSSION

A. Simulation Setup and Comparative Technical Performance

The proposed feasibility-aware PV BESS co-planning framework is evaluated on the 33 bus and 69 bus radial DNs over a 24 hour scheduling horizon. Three PV units and one BESS are jointly optimized in each system. The network characteristics, planning limits, and BESS operating parameters are summarized in Table 2, while the hourly load and PV profiles and time-of-use electricity tariffs are presented in Tables 4–6.

Tables 4–6 summarize the normalized hourly load demand, PV generation profiles, and TOU electricity tariffs adopted in the deterministic 24 hour simulation. The load and PV factors are applied to the nominal bus demands and installed PV capacities, respectively. For hourly intervals crossing the tariff transition times of 09:30 and 11:30, a time weighted average tariff is used to calculate electricity purchasing expenditure. The aggregate load and PV profile factors over the 24-hour horizon are 19.94 and 7.88, respectively, ensuring consistent

application of the input profiles across all investigated cases.

Table 4. Normalized Hourly Load Demand Profile

Hour	Load factor	Hour	Load factor	Hour	Load factor
1	0.63	9	0.87	17	0.98
2	0.60	10	0.91	18	0.96
3	0.58	11	0.94	19	0.99
4	0.57	12	0.93	20	1.00
5	0.60	13	0.91	21	0.96
6	0.68	14	0.94	22	0.88
7	0.76	15	0.97	23	0.78

Table 5. Normalized Hourly Photovoltaic Generation Profile

Hour	PV factor	Hour	PV factor	Hour	PV factor
1	0.00	9	0.64	17	0.38
2	0.00	10	0.82	18	0.15
3	0.00	11	0.93	19	0.00
4	0.00	12	1.00	20	0.00
5	0.02	13	0.96	21	0.00
6	0.08	14	0.90	22	0.00
7	0.20	15	0.78	23	0.00
8	0.42	16	0.60	24	0.00

The comparative evaluation considers accommodated PV capacity, daily energy losses, minimum bus voltage, maximum branch current, renewable energy utilization, upstream grid imports, and daily electricity purchasing expenditure. The optimization algorithms are implemented using the common settings provided in Table 3, while the network and PV–BESS simulation parameters are summarized in Table 2. A uniform branch current limit of 255 A is adopted as a simulation assumption for both test systems.

Table 6. Time of use Electricity Tariff

Period	Time interval	Tariff (USD/kWh)
Off-peak	22:00–04:00	0.0425
Normal	04:00–09:30; 11:30–17:00; 20:00–22:00	0.0665
Peak	09:30–11:30; 17:00–20:00	0.1183

B. Results for the 33 bus System

Figure 1 presents the single line diagram of the 33 bus DN, which consists of 33 buses and 32 branches with a total peak demand of 3.715 MW and 2.300 MVAr [24], [25]. The line and load data follow Baran and Wu [25]; at unity load factor, the base case power flow solution gives 202.7 kW of losses and a minimum voltage of 0.9131 p.u. at bus 18, matching the benchmark values. As shown in Table 7, all four algorithms locate feasible configurations that use the full aggregate PV limit or nearly so. The lowest objective value among the best runs is obtained by ARO (F = 0.2953), followed by DE (0.2954); the best MVO run gives 0.3034. The ARO solution places PV units at buses 7, 31, 14 (2.850 MW) and a 1.350 MWh BESS at bus 16, reducing the daily feeder loss from 3.405 to 2.280 MWh (33.0%) with a PV utilization of 99.97%. The lowest daily loss is obtained by DE (2.221 MWh), and the MVO solution reduces the loss to 2.343 MWh (31.2%). The maximum branch current remains below the assumed 255 A limit for all solutions. The minimum voltage over the day changes only marginally (0.9131 p.u. in the base case) because it occurs at the evening peak, when PV

output is zero and the unity power factor BESS discharge is limited by its converter rating; all voltages remain within 0.90–1.05 p.u.

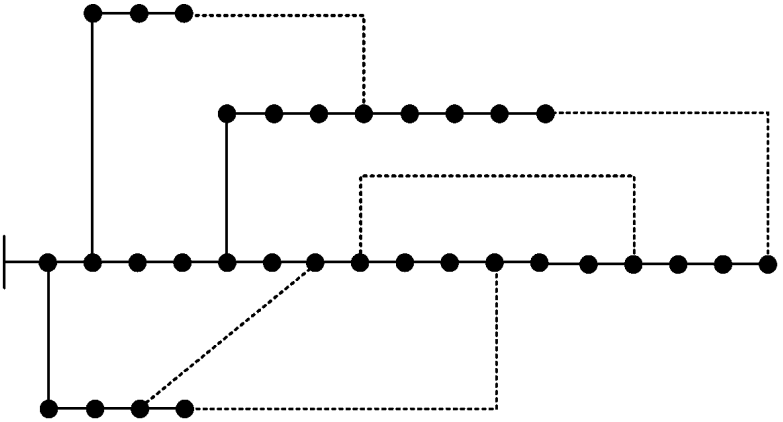


Figure 1. Diagram of the 33 bus DN

Table 7. Comparative Technical Performance for the 33 bus Distribution Network

Parameter	Base Case	DE	HHO	ARO	MVO
PV installation buses	–	6, 31, 14	26, 31, 11	7, 31, 14	14, 7, 31
PV capacities (MW)	–	0.950, 0.950, 0.942	0.950, 0.950, 0.950	0.950, 0.950, 0.950	0.950, 0.950, 0.950
BESS bus	–	14	19	16	2
BESS capacity (MWh)	–	1.800	1.800	1.350	1.048
Daily energy loss (MWh)	3.405	2.221	2.365	2.280	2.343
Minimum voltage over 24 h (p.u.)	0.9131	0.9173	0.9132	0.9142	0.9131
Accommodated PV capacity (MW)	–	2.842	2.850	2.850	2.850
PV utilization (%)	–	98.17	98.98	99.97	98.40
Maximum branch current (A)	210.4	202.5	228.5	209.2	209.7
Upstream energy import (MWh/day)	77.482	54.458	54.493	53.995	54.459
TOU purchasing expenditure (USD/day)	5,773	3,942	3,957	3,914	3,935
f1	1.0000	0.6521	0.6944	0.6694	0.6880
f2	1.0000	0.6846	0.6992	0.6752	0.6796
f3	–	0.0029	0.0000	0.0000	0.0000
f4	–	0.0183	0.0102	0.0003	0.0160
f5	0.1613	0.1310	0.1368	0.1334	0.1353
Objective F (Eq. 17)	–	0.2954	0.3074	0.2953	0.3034
Constraint violation CV (Eq. 30)	–	0.0000	0.0000	0.0000	0.0000
Hours with V outside 0.90–1.05 p.u.	0	0	0	0	0
Feasible (CV ≤ 1e-7)	–	Yes	Yes	Yes	Yes

Daily upstream grid imports decrease from 77.482 MWh to between 53.995 and 54.493 MWh, and the daily grid electricity purchasing expenditure decreases from USD 5,773 to USD 3,914 for the ARO solution (32.2%) and to USD 3,935 for the MVO solution (31.8%) under the adopted time-of-use tariff. These values include the BESS conversion losses, which are reported in the energy balance of Table 9.

Figure 2 illustrates the 24 hour operation of the best MVO configuration for the 33 bus DN, which is used here as the reference solver; the hourly results of the other solutions are archived in the Supplementary Data workbook. Figure 2(a) compares the bus voltage profiles

before and after PV BESS integration at the peak load hour 20, together with the 24 hour minimum and maximum envelopes. During the PV hours, the minimum feeder voltage rises from about 0.92 p.u. in the base case to about 0.98 p.u. at hours 10–13, while the maximum voltage over the day does not exceed 1.0002 p.u., so no overvoltage occurs. At hour 20, when PV output is zero, the minimum voltage at bus 18 remains 0.9131 p.u., which confirms that the evening peak is the binding operating condition. Figure 2(b) shows the BESS charging/discharging power and the SOC trajectory. The battery, located at bus 2 near the substation, charges mainly during the off-peak early morning hours and partly during the PV hours, and discharges around midday and in the evening; its SOC varies between 0.24 and 0.80, remains within the 0.20–0.90 limits, and returns to 0.50 at the end of the day, satisfying the cyclic condition (16). Because of its location close to the substation, the BESS has only a minor influence on the feeder voltages and losses. Figure 2(c) compares the available and utilized PV power; curtailment is small (0.358 MWh/day, 1.6% of the available energy) and occurs mainly at hours 6 and 14. Figure 2(d) shows the hourly feeder losses: the loss reduction of 1.063 MWh/day is obtained almost entirely during the PV hours, whereas the evening losses (about 200 kW at hours 19–20) are practically unchanged. The totals of the hourly values equal the daily quantities reported in Tables 7 and 9.

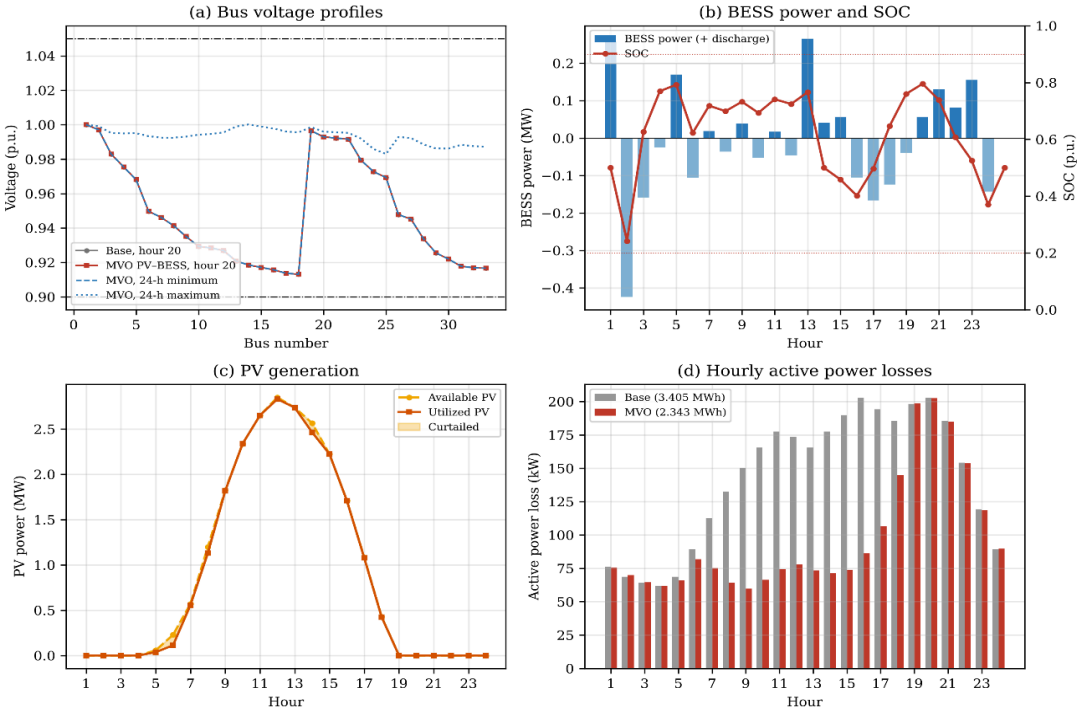


Figure 2. Operational performance of the 33 bus DN: (a) voltage profiles, (b) BESS charging/discharging power and SOC, (c) PV generation profiles, and (d) hourly active power losses.

C. Results for the 69 bus System

Figure 3 illustrates the complete single line diagram of the 69 bus radial DN, comprising 69 buses and 68 branches with a total peak demand of 3.802 MW and 2.694 MVAr [25], [26]. At unity load factor, the base case losses are 225.0 kW and the minimum voltage is 0.9092 p.u. at bus 65. This larger benchmark is used to evaluate the framework under a different topology and load distribution. The comparative technical results are summarized in Table 8.

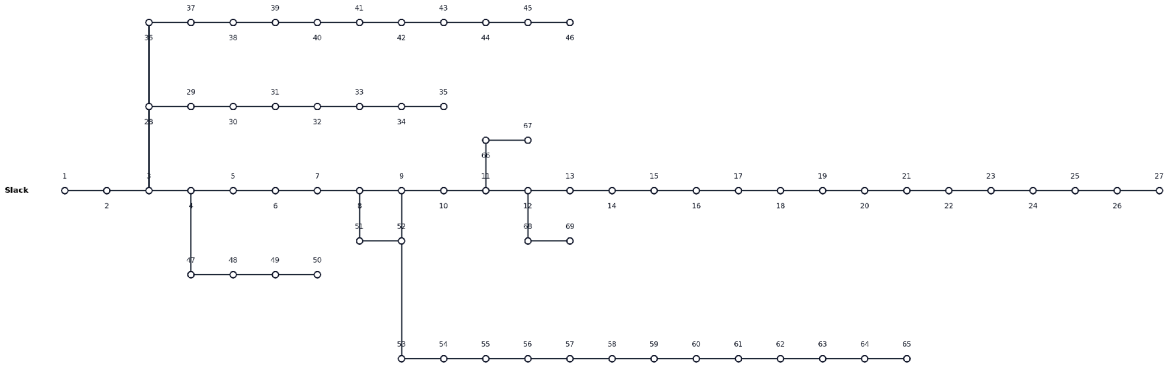


Figure 3. Diagram of the 69 bus DN.

Table 7. Comparative Technical Performance for the 33 bus Distribution Network

Parameter	Base Case	DE	HHO	ARO	MVO
PV installation buses	–	61, 14, 62	13, 61, 63	61, 62, 14	61, 62, 14
PV capacities (MW)	–	1.100, 1.095, 1.095	1.100, 1.100, 1.100	1.100, 1.100, 1.100	1.100, 1.099, 1.100
BESS bus	–	61	30	18	50
BESS capacity (MWh)	–	2.000	0.214	0.200	0.217
Daily energy loss (MWh)	3.768	2.344	2.605	2.467	2.494
Minimum voltage over 24 h (p.u.)	0.9092	0.9113	0.9092	0.9094	0.9092
Accommodated PV capacity (MW)	–	3.290	3.300	3.300	3.299
PV utilization (%)	–	98.20	91.70	99.94	95.75
Maximum branch current (A)	223.6	216.2	223.5	222.1	223.4
Upstream energy import (MWh/day)	79.584	52.909	54.597	52.336	53.426
TOU purchasing expenditure (USD/day)	5,930	3,778	3,913	3,761	3,849
f1	1.0000	0.6221	0.6913	0.6546	0.6618
f2	1.0000	0.6198	0.6586	0.6160	0.6352
f3	–	0.0031	-0.0000	-0.0000	0.0002
f4	–	0.0180	0.0830	0.0006	0.0425
f5	0.1398	0.1144	0.1191	0.1160	0.1166
Objective F (Eq. 17)	–	0.2749	0.3079	0.2794	0.2905
Constraint violation CV (Eq. 30)	–	0.0000	0.0000	0.0000	0.0000
Hours with V outside 0.90–1.05 p.u.	0	0	0	0	0
Feasible (CV ≤ 1e-7)	–	Yes	Yes	Yes	Yes

As shown in Table 8, all four algorithms locate feasible configurations that use the full aggregate PV limit or nearly so. The lowest objective value among the best runs is obtained by DE (F = 0.2749), followed by ARO (0.2794); the best MVO run gives 0.2905. The DE solution places PV units at buses 61, 14, 62 (3.290 MW) and a 2.000 MWh BESS at bus 61, reducing the daily feeder loss from 3.768 to 2.344 MWh (37.8%) with a PV utilization of 98.20%. The lowest daily loss is obtained by DE (2.344 MWh), and the MVO solution reduces the loss to 2.494 MWh (33.8%). The maximum branch current remains below the assumed 255 A limit for all solutions. The minimum voltage over the day changes only marginally (0.9092 p.u. in the base case) because it occurs at the evening peak, when PV output is zero and the unity-power-factor BESS discharge is limited by its converter rating; all voltages remain within 0.90–1.05 p.u. Daily upstream grid imports decrease from 79.584 MWh to between 52.336 and 54.597 MWh, and the daily grid electricity purchasing expenditure decreases from USD 5,930 to USD 3,778 for the DE solution (36.3%) and to USD 3,849 for the MVO solution (35.1%) under the adopted time-of-use tariff. These values

include the BESS conversion losses, which are reported in the energy balance of Table 9.

Table 9. Energy Balance and Operating Cost for the 33 bus and 69 bus Systems

Parameter	33-bus Base	33-bus MVO	69-bus Base	69-bus MVO
Load	74.0771	74.0771	75.8157	75.8157
Loss	3.4053	2.3427	3.7681	2.4939
PV available	0	22.458	0	26.000
PV used	0	22.0997	0	24.8951
PV curtailed	0	0.3583	0	1.1049
BESS charge	0	1.4267	0	0.1169
BESS discharge	0	1.2876	0	0.1055
BESS loss	0	0.1391	0	0.0114
Grid import	77.48	54.46	79.58	53.43
Grid export	0	0	0	0
Cost (USD)	5,773	3,935	5,930	3,849
Residual	0	0	0	0

Figure 4 presents the corresponding 24 hour operation of the best MVO configuration for the 69-bus DN, discussed in detail below.

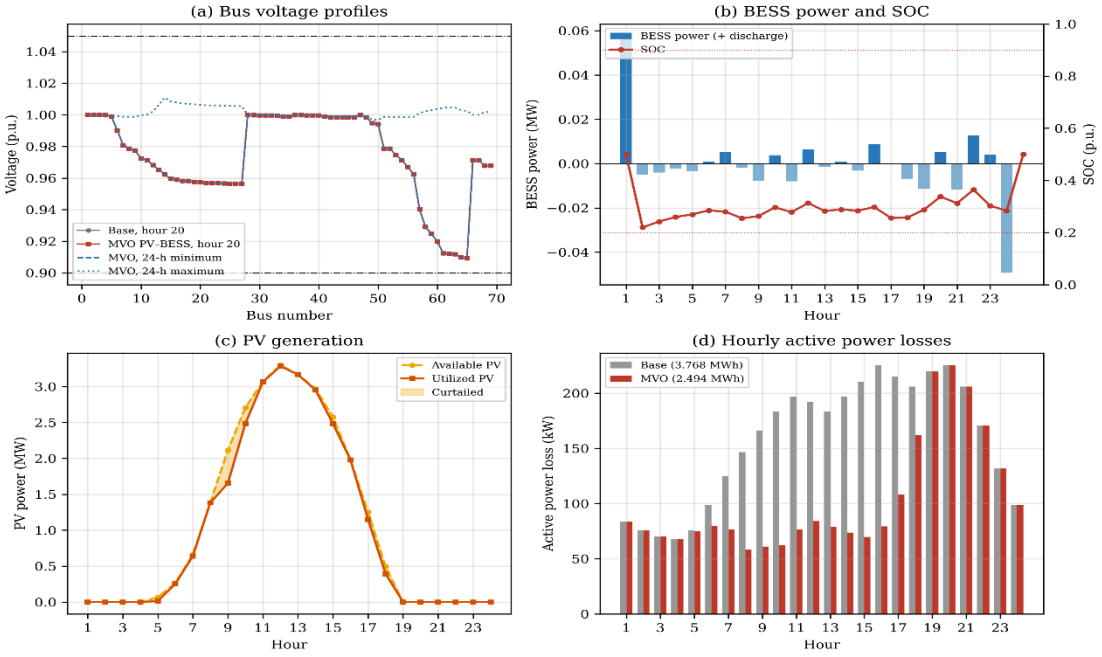


Figure 4. Operational performance of the 69 bus DN: (a) voltage profiles, (b) BESS charging/discharging power and SOC, (c) PV generation profiles, and (d) hourly active power losses.

Table 9 verifies the daily energy balance of the base case and the best MVO solutions: for every case, the net grid import (import minus export) equals the load demand plus feeder losses minus the utilized PV energy plus the BESS conversion losses, and the residual is zero within the displayed precision. Because the BESS operates cyclically with charging and discharging efficiencies of 95%, the energy drawn for charging exceeds the energy returned during discharge. The difference, 0.139 MWh/day for the 33-bus system and 0.011 MWh/day for the 69-bus system, is supplied by the network and is therefore included in the reported grid imports and daily purchasing expenditure. The small value for the 69-bus system reflects the low energy rating (0.217 MWh) of the BESS in the best MVO solution.

Figure 4 presents the corresponding 24 hour operation of the best MVO configuration for the 69-bus DN. Figure 4(a) shows the voltage profiles at the peak load hour 20 together with the 24 hour minimum and maximum envelopes. During the PV hours, the minimum feeder voltage rises from about 0.915 p.u. in the base case to about 0.995 p.u. at hours 11–13, and the maximum voltage reaches 1.011 p.u. at hour 12, remaining below the 1.05 p.u. limit. At hour 20, the minimum voltage at bus 65 remains 0.9092 p.u., as in the base case, confirming again that the evening peak is the binding operating condition. Figure 4(b) shows that the BESS selected in this solution is small (0.217 MWh at bus 50) and operates with low power, below 0.06 MW in magnitude; its SOC varies between 0.22 and 0.50, stays within the 0.20–0.90 limits, and returns to 0.50 at the end of the day, satisfying the cyclic condition (16). This indicates that, for the 69-bus system, the objective is improved mainly through PV siting and sizing rather than through energy shifting by the BESS. Figure 4(c) compares the available and utilized PV power; curtailment amounts to 1.105 MWh/day (4.2% of the available energy) and is concentrated at hours 9–10. Figure 4(d) shows that the loss reduction of 1.274 MWh/day occurs entirely during the PV hours, whereas the evening losses (about 225 kW at hours 19–20) are practically unchanged. The PV and hourly loss profiles sum to the daily values reported in Tables 8 and 9.

D. Statistical Performance and Feasibility Assessment

The results in Tables 7 and 8 correspond to the best run of each algorithm and therefore do not reflect the variability of stochastic search. To assess the robustness of the compared methods and of the proposed constraint-handling procedure, the outcomes of all 30 independent runs are analyzed for both test systems. Table 10 reports the number of feasible runs and the descriptive statistics of the objective value F, Table 11 presents the Holm-adjusted Mann–Whitney tests between MVO and each competing algorithm, and Table 12 summarizes an ablation analysis that isolates the contributions of cyclic BESS repair and feasibility-first selection.

Table 10. Statistical performance comparison of DE, HHO, ARO, and MVO

Parameter	33 DE	33 HHO	33 ARO	33 MVO	69 DE	69 HHO	69 ARO	69 MVO
Feasible	30/30	30/30	30/30	30/30	30/30	30/30	30/30	30/30
Fbest	0.2954	0.3074	0.2953	0.3034	0.2749	0.3079	0.2794	0.2905
Fmean	0.3018	0.3688	0.3002	0.3127	0.2847	0.3904	0.2866	0.3037
Fmedian	0.3008	0.3656	0.2998	0.3117	0.2828	0.4038	0.2831	0.3005
Fworst	0.3188	0.4383	0.3054	0.3333	0.3031	0.4698	0.3098	0.3356
Fstd	0.0048	0.0337	0.0022	0.0076	0.0070	0.0464	0.0087	0.0111
CVbest	6.39E-12	4.97E-11	1.03E-10	2.69E-11	1.72E-12	4.82E-11	6.39E-11	1.69E-11
CVmean	7.91E-10	9.41E-10	1.44E-09	5.73E-10	7.42E-10	1.21E-09	9.04E-10	7.08E-10
CVmedian	4.72E-10	4.62E-10	6.12E-10	5.30E-10	3.73E-10	5.02E-10	6.12E-10	5.38E-10
CVworst	4.66E-09	4.83E-09	4.88E-09	1.55E-09	3.35E-09	4.13E-09	3.42E-09	4.29E-09
CVstd	1.15E-09	1.15E-09	1.46E-09	3.91E-10	9.10E-10	1.24E-09	8.27E-10	8.34E-10
Time (s)	6.99	6.90	6.42	7.17	7.96	7.97	7.45	8.26

Table 10 summarizes the objective values of DE, HHO, ARO, and MVO over 30 independent runs. All runs of all algorithms are feasible under the adopted limits, so the statistics are computed over 30 feasible runs. For the 33-bus system, ARO and DE yield the lowest and nearly equal mean objective values (0.3002 and 0.3018), followed by MVO (0.3127) and HHO (0.3688); ARO also attains the lowest single best value (0.2953). For the 69-bus system, DE and ARO again yield the lowest and nearly equal mean values (0.2847 and 0.2866), followed by MVO (0.3037) and HHO (0.3904); DE attains the lowest single best value (0.2749). Thus, DE and ARO perform best within the proposed framework and show small dispersions, MVO ranks third with a consistent but slightly higher objective, and HHO exhibits the largest dispersion under the common budget. Mean computation times are similar for all methods because the run time is dominated by the 3,000 hourly power flow evaluations.

Table 11. Statistical Significance of MVO compared with the Competing Algorithms

Comparison	33-bus adjusted p-value	69-bus adjusted p-value
MVO vs. DE	1.85×10^{-8}	2.20×10^{-8}
MVO vs. HHO	1.62×10^{-9}	8.61×10^{-10}
MVO vs. ARO	1.82×10^{-10}	3.26×10^{-7}

As shown in Table 11, all Holm adjusted p-values are below 0.05 for both systems. Relative to MVO, the mean objective is lower for DE by 3.5% and 6.3% and for ARO by 4.0% and 5.6% on the 33 bus and 69 bus systems, respectively, whereas MVO improves on HHO by 15.2% and 22.2%. Hence, within the investigated budget, the feasibility aware framework is more effective with DE or ARO than with MVO. Because the constraint-handling workflow is independent of the search operators, these results support its use with different metaheuristics; they do not imply global optimality or general superiority of any algorithm in other operating scenarios.

Table 12 evaluates the contributions of cyclic BESS dispatch repair and feasibility first selection. Without cyclic repair, the terminal-energy equality (16) is never met to the feasibility tolerance, so conventional MVO and MVO with feasibility first selection alone yield 0 and 0 feasible runs for the 33 bus system (0 and 0 for the 69-bus system), although the residual terminal SOC errors are small. With cyclic repair, the terminal error is reduced to the numerical tolerance and 30/30 and 30/30 runs are feasible; the complete framework yields 30/30 and 30/30. The mean feasible objective values of the two configurations with cyclic repair are similar (0.3107 versus 0.3127 for the 33-bus system and 0.3072 versus 0.3037 for the 69-bus system). Because no network violations occur under the 0.90–1.05 p.u. band, cyclic repair is the decisive component for battery feasibility, whereas feasibility-first selection acts as a safeguard that becomes relevant when voltage or thermal limits are binding.

Table 12. Ablation Analysis of the Feasibility-aware MVO Framework

Configuration	33 bus Feasible	33 bus Mean F	33 bus Mean CV	69 bus Feasible	69 bus Mean F	69 bus Mean CV
Conventional MVO	0/30	0.4472	6.34E-05	0/30	0.4594	6.75E-05
MVO + cyclic repair	30/30	0.3107	5.86E-10	30/30	0.3072	7.27E-10
MVO + feasibility-first	0/30	0.5883	2.77E-05	0/30	0.6125	2.29E-05
Complete framework	30/30	0.3127	5.73E-10	30/30	0.3037	7.08E-10

E. Operational Analysis and Technical Discussion

The operational results in Figures 2 and 4 illustrate the effects of coordinated PV BESS integration on bus voltage profiles, battery charging/discharging schedules, SOC trajectories, PV generation, and hourly feeder losses in the 33 bus and 69 bus DNs, respectively. The BESS schedules are subject to charging/discharging power limits, SOC constraints, and daily cyclic energy requirements, while hourly BFS power flow calculations are used to evaluate voltage and branch current constraints. The results show that coordinated PV BESS planning reduces losses and grid imports mainly during the PV hours, whereas the evening minimum voltage remains the binding operating condition; without reactive power support, the unity power factor BESS can raise this voltage only marginally. The economic assessment considers daily grid electricity purchasing expenditure under the adopted time of use tariffs. As reported in Tables 7 and 8, all optimized configurations achieve lower purchasing expenditure than the corresponding base cases. However, this indicator excludes BESS investment, maintenance, degradation, replacement, and other life cycle costs. Therefore, the reported expenditure reductions should be interpreted as operational electricity purchasing benefits rather than comprehensive economic savings.

CONCLUSION

This paper presented a feasibility aware PV BESS co-planning framework integrating coordinated siting and sizing, 24 hour battery scheduling, cyclic dispatch repair, and hourly network feasibility assessment. The framework was evaluated on the 33 bus and 69 bus radial DNs using Baran–Wu data, a 0.90–1.05 p.u. voltage band, and 30 independent runs of four metaheuristics. All runs are feasible, and the best solutions accommodate up to the PV planning limits of 2.85 MW and 3.30 MW. The lowest-objective solutions (ARO and DE) reduce daily feeder losses from 3.405 to 2.280 MWh (33.0%) and from 3.768 to 2.344 MWh (37.8%), with renewable energy utilization of 99.97% and 98.20%, and decrease the TOU purchasing expenditure by 32.2% and 36.3%, including BESS conversion losses. ARO and DE achieve the lowest mean objective values on the 33 bus and 69 bus systems, respectively, with statistically significant differences, while MVO outperforms only HHO. The ablation analysis shows that cyclic BESS repair is essential for satisfying the terminal-energy condition. With unity-power-factor units, the evening peak limits the achievable minimum voltage. The reported accommodated PV capacities are the best feasible solutions identified within the computational budget rather than certified HC limits. Future research will investigate inverter reactive power support, renewable generation uncertainty, battery degradation, and life cycle economic assessment.

REFERENCES

[1] S. M. Sadek, A. A. Hassan, F. H. Fahmy, A. A. El-deib, and H. K. M. Youssef, “Photovoltaic hosting capacity assessment in distribution networks,” J. Electr. Syst. Inf. Technol., vol. 12, 2025, doi: 10.1186/s43067-025-00296-9.

[2] H. H. H. Mousa, K. Mahmoud, and M. Lehtonen, “A Comprehensive Review on Recent Developments of Hosting Capacity Estimation and Optimization for Active Distribution Networks,” IEEE Access, vol. 12, pp. 18545–18593, 2024, doi: 10.1109/ACCESS.2024.3359431.

[3] A. Baniasadi, D. Habibi, W. Al-saedi, M. A. S. Masoum, and C. K. Das, “Optimal sizing design and operation of electrical and thermal energy storage systems in smart buildings,” J. Energy Storage, vol. 28, p. 101186, 2020, doi: 10.1016/j.est.2019.101186.

[4] C. K. Das, O. Bass, T. S. Mahmoud, G. Kothapalli, M. A. S. Masoum, and N. Mousavi, “An optimal allocation and sizing strategy of distributed energy storage systems to improve performance of distribution networks,” J. Energy Storage, vol. 26, p. 100847, 2019, doi: 10.1016/j.est.2019.100847.

[5] I. U. Salam, M. Yousif, M. Numan, K. Zeb, and M. Billah, “Optimizing Distributed Generation Placement and Sizing in Distribution Systems: A Multi-Objective Analysis of Power Losses, Reliability, and Operational Constraints,” Energies, vol. 16, no. 16, p. 5907, 2023, doi: 10.3390/en16165907.

[6] F. K. Ariyo, A. P. Adeagbo, O. B. Adewuyi, S. O. Ayanlade, and T. U. Badrudeen., “Advanced particle swarm optimization for efficient coordination of distributed generators in power distribution networks,” J. Electr. Syst. Inf. Technol., vol. 12, no. 39, 2025, doi: 10.1186/s43067-025-00231-y.

[7] L. H. Thai and T. N. Ton, “Optimizing Renewable Integration in Distribution Power Systems Using an Improved Artificial Bee Colony Algorithm,” Eng. Technol. Appl. Sci. Res., vol. 15, no. 4, pp. 25270–25274, 2025, doi: 10.48084/etasr.12316.

[8] T. N. Ton, P. M. Le, L. H. Pham, and T. M. Le, “Bi-Level DG Optimization in Distribution Networks with TOU Pricing and Demand Response Using MPA,” ECTI Trans. Electr. Eng. Electron. Commun., vol. 23, no. 3, pp. 1–10, 2025, doi: 10.37936/ecti-eec.2525231.259805.

[9] R. Ahmad, N. Gupta, K. R. Niazi, A. Swarnkar, and N. K. Meena, “Estimation of State-of-Charge for Dynamic Management of Battery Energy Storage Systems for High

Renewable Penetration," Int. Conf. Power Electron. IoT Appl. Renew. Energy its Control, pp. 96–101, 2020, doi: 10.1109/PARC49193.2020.236565.
[10] K. Lee, P. Zhao, A. Bhattacharya, B. K. Mallick, and L. Xie, "An Active Learning-based Approach for Hosting Capacity Analysis in Distribution Systems," IEEE Trans. Smart Grid, vol. 15, no. 1, pp. 617–626, 2024, doi: 10.1109/TSG.2023.3290414.
[11] V. K. Thunuguntla, V. Maineni, and S. K. Injeti, "A TOPSIS based multi-objective optimal deployment of solar PV and BESS units in power distribution system electric vehicles load demand," Sci. Rep., vol. 14, no. 29688, pp. 1–18, 2024, doi: 10.1038/s41598-024-79519-4.
[12] M. A. Hannan et al., "Battery energy-storage system: A review of technologies, optimization objectives, constraints, approaches, and outstanding issues," J. Energy Storage, vol. 42, p. 103023, 2021, doi: 10.1016/j.est.2021.103023.
[13] A. Kharrazi, V. Sreeram, and Y. Mishra, "Assessment techniques of the impact of grid-tied rooftop photovoltaic generation on the power quality of low voltage distribution network - A review," Renew. Sustain. Energy Rev., vol. 120, p. 109643, 2020, doi: 10.1016/j.rser.2019.109643.
[14] I. Cetinbas, B. Tamyurek, and M. Demirtas, "The Hybrid Harris Hawks Optimizer-Arithmetic Optimization Algorithm: A New Hybrid Algorithm for Sizing Optimization and Design of Microgrids," IEEE Access, vol. 10, pp. 19254–19283, 2022, doi: 10.1109/ACCESS.2022.3151119.
[15] Venkata Anjani Kumar G, M. Damodar Reddy, Chilakapati Lenin Babu, and Palepu Suresh Babu, "Performance Assessment of a Multi-Verse Optimizer-Based Solar-PV Inverter for Grid-Connected Applications," J. Eng. Technol. Ind. Appl., vol. 11, no. 51, pp. 151–156, 2025, doi: 10.5935/jetia.v11i51.1334.
[16] B. Venkatanarayana and K. M. Rosalina, "A new MPPT mechanism based on multi-verse optimization algorithm tuned FLC for photovoltaic systems," Sci. Rep., vol. 14, no. 28066, pp. 1–17, 2024, doi: 10.1038/s41598-024-79554-1.
[17] N. Karuppiah, J. S. S. Muthubalaji, and L. M, "Optimal siting and sizing of multiple type DGs for the performance enhancement of Distribution System using Differential Evolution Algorithm," Turkish J. Comput. Math. Educ., vol. 12, no. 2, pp. 1140–1146, 2021, doi: 10.17762/turcomat.v12i2.1135.
[18] M. Fan, J. Chen, Z. Xie, H. Ouyang, S. Li, and L. Gao, "Improved multi - objective differential evolution algorithm based on a decomposition strategy for multi - objective optimization problems," Sci. Rep., vol. 12, no. 29006, pp. 1–14, 2022, doi: 10.1038/s41598-022-25440-7.
[19] H. M. Alabool, D. Alarabiat, L. Abualigah, and A. A. Heidari, "Harris hawks optimization: a comprehensive review of recent variants and applications," Neural Comput. Appl., vol. 33, no. 15, pp. 8939–8980, 2021, doi: 10.1007/s00521-021-05720-5.
[20] A. Selim, S. Kamel, A. S. Alghamdi, and F. Jurado, "Optimal Placement of DGs in Distribution System Using an Improved Harris Hawks Optimizer Based on Single- And Multi-Objective Approaches," IEEE Access, vol. 8, pp. 52815–52829, 2020, doi: 10.1109/ACCESS.2020.2980245.
[21] Chegudi Ranga Rao, Ramadoss Balamurugan, and RamaKoteswaraRao Alla, "Artificial Rabbits Optimization Based Optimal Allocation of Solar Photovoltaic Systems and Passive Power Filters in Radial Distribution Network for Power Quality Improvement," Int. J. Intell. Eng. Syst., vol. 16, no. 1, pp. 100–109, 2023, doi: 10.22266/ijies2023.0228.09.
[22] H. Jia, Y. Su, H. Rao, M. Liang, and L. Abualigah, "Improved artificial rabbits algorithm for global optimization and multi-level thresholding color image segmentation," Artif. Intell. Rev., vol. 58, no. 55, 2025, doi: 10.1007/s10462-024-11035-3.
[23] S. R. Biswal, G. Shankar, R. M. Elavarasan, and L. Mihet-Popa, "Optimal Allocation/Sizing of DGs/Capacitors in Reconfigured Radial Distribution System Using Quasi-Reflected Slime Mould Algorithm," IEEE Access, vol. 9, pp. 125658–125677, 2021, doi: 10.1109/ACCESS.2021.3111027.

[24] T. N. Ton, P. M. Le, and T. M. Le, “Multi-objective optimization of distributed generation placement and sizing in active distribution networks considering harmonic distortion,” Int. J. Electr. Comput. Eng., vol. 16, no. 2, pp. 598–607, 2026, doi: 10.11591/ijece.v16i2.pp598-607.
[25] M. E. Baran and F. F. Wu, “Network reconfiguration in distribution systems for loss reduction and load balancing,” IEEE Trans. Power Deliv., vol. 4, no. 2, pp. 1401–1407, 1989, doi: 10.1109/61.25627.
[26] T. N. Ton, H. H. Lai, L. V. Pham, and T. N. Hoang, “Optimization of Distributed Generation Planning to Maximize the Absorption Rate of Renewable Energy in Distribution Networks,” Eng. Technol. Appl. Sci. Res., vol. 15, no. 3, pp. 23008–23013, 2025, doi: 10.48084/etasr.10921.

BIOGRAPHY OF AUTHOR



Trieu Ngoc Ton was born in Quang Ngai, Vietnam, in 1981. He received the B.Eng., M.Eng., and Ph.D. degrees in Electrical Engineering from Ho Chi Minh City University of Technology and Education, Vietnam, in 2005, 2009, and 2023, respectively. He is currently a lecturer in the Faculty of Electrical and Electronics Engineering at Thu Duc College of Technology, Ho Chi Minh City, Vietnam. His research interests include power distribution systems, distributed generation optimization, renewable energy integration, and energy storage systems.